Attachment 2 to
AECM-84/0373

METALLURGICAL EVALUATION

OF

DIESEL GENERATOR TURBOCHARGER

GUIDE VANE HOLD DOWN BOLTS

AT

GRAND GULF NUCLEAR STATION - UNIT 1

PREPARED FOR: NUCLEAR PLANT ENGINEERING
MISSISSIPPI POWER & LIGHT COMPANY
PORT GIBSON, MISSISSIPPI 39150

PREPARED BY: J. S. BRIHMADESAM
NUCLEAR ENGINEERING DEPARTMENT
MIDDLE SOUTH SERVICE, INC.
NEW ORLEANS, LOUISIANA 70112

JULY, 1984

TABLE OF CONTENTS

LIST OF FIGURES

LIST OF FIGURES
(CONTINUED)

1.0 INTRODUCTION

1.1 General

Inspection of the Division I Diesel Generator Turbocharger during the NRC mandated[1] teardown of the diesel engine (May - June 1984) revealed that two bolts on one turbocharger had broken off and were missing. The lockwire securing these bolts was also broken. On the other turbocharger one bolt had broken off but was held in place by the lockwire. The remaining six bolts on the first turbocharger and seven bolts on the second were intact and showed no evidence of cracking. A similar inspection of the Division II diesel engine turbocharger revealed no such damage. The bolt material was determined to be A-286 stainless steel (see Section 5 for chemical analysis).

1.2 History

The turbochargers on Division I diesel engine were replaced during maintenance operations on the engine in September 1983. The replacement turbochargers were obtained from Grand Gulf-Unit 2 engines which were in a warehouse. It is believed that these turbochargers had about 30 hours of operation at the factory and had subsequently been in storage for a period of four to six years. Exact storage conditions could not be ascertained. These turbochargers, after installation on Division I engine, had experienced a total of 572 hours of operational time and 119 starts during that time.

The turbochargers on Division II diesel engine are original equipment and had a total operational time of 900 hours and 128 starts.

2.0 VISUAL EXAMINATION

The broken bolt head and the intact bolts from both Division I and Division II diesel engines were visually examined under a low power stereo-microscope. The bolts had a reddish oxide deposit in areas exposed to

2.0 (CONTINUED)

exhaust gases. On some bolts there was a whitish salt-like deposit at the head to shank radius. Some bolts also had a small ridge of reddish brown oxide at the interface between nozzel ring and turbocharger body. These observed features are shown in Figure 1. The fracture surface of the broken bolt showed a smooth half moon surface and a grainy morphology elsewhere. A macrograph of the fracture surface is shown in Figure 2. Lower power microscopic evaluation of the bolts did not reveal the presence of cracks in any of the other bolts and the fracture surface of the broken bolt showed evidence of secondary cracking in the grainy region.

3.0 METALLOGRAPHY

Metallography was performed on the following specimens:

1. Cross-section of the broken bolt from Division I turbocharger.
2. Cross-section of a good bolt from Division I turbocharger.
3. Cross-section of a good unused bolt.
4. Cross-section from four bolts from Division I turbocharger (two each from right and left banks identified as R2, R6, L1 and L3).
5. A washer from Division II turbocharger.

3.1 Broken Bolt

A cross-section, as shown in Figure 2, was obtained, polished and etched. The crack profile is shown in Figure 3. The crack is intergranular and appears to be filled with corrosion products. In order to determine the morphology and identify the corrosion products, this cross-section was further analyzed using a Scanning Electron Microscope (SEM). SEM metallographs are presented in Figures 4 through 8. Figure 4 is taken at the fracture surface showing the individual grains, secondary cracking and a profile of secondary cracks on the polished face. Figure 5 shows the existence of the branched intergranular cracks which connect to other cracks that

3.1 (CONTINUED)

emanate from the fracture surface. Intermetallic precipitates, primarily titanium and molybdenum, are also evident. At a higher magnification, Figure 6, the corrosion product within the grain boundaries is clearly visible. The corrosion product was identified to be predominantly iron with no evidence of sulphur. Thus, the product being iron oxide. This aspect is further discussed in Section 5, Chemical Analysis. Figure 7 shows the attack at the grain boundary and the remanant of a precipitate. The precipitate was found to be mostly titanium. Figure 8 shows a grain boundary corrosion product deposit with evidence of a whitish phase along the grain boundary. This whitish phase was found to be a nickel rich phase. The chemical identification of the corrosion products and phases identified here are presented in Section 5.

3.2 Microstructure Comparisons

The microstructures of Division I turbocharger bolts (one broken plus one unbroken) are shown in Figures 9 through 12. Figure 13 is a micrograph of an unusual bolt. Figures 9 and 10 show evidence of intermetallic precipitates, some grain boundary precipitates and large austenite grains. Figures 11 and 12, at a higher magnification show the grain boundary precipitation more clearly. Figure 13, micrograph of an unused bolt, is taken at a slightly higher magnification than those in Figures 9 and 10. A comparison between these three figures clearly shows that the bolts in Division I turbocharger had significantly larger grains and were sensitized (i.e., grain boundary carbide precipitation). Also, comparing Figures 9 and 10 to the photo micrographs in Reference 1 a similar observation is evident.

The microstructures of Division II turbocharger bolts are shown in Figures 14 through 19. Figures 14 through 17 are micrographs at 400x on each of the four bolts (L1, L3, R2 and R6). A comparison between these microstructures and those shown in Figures 9 and 10 clearly show

3.2 (CONTINUED)

that the Division I turbocharger bolts had significantly larger austenite grains. The bolts from the Division II turbocharger had seen longer operational time and similar operating conditions (i.e., exhaust gas temperatures). Therefore it is clear that the larger grainsize in Division I turbocharger was due to the heat treatment process rather than a service induced condition. Figures 18 and 19 are a higher magnification micrograph of bolts L3 and R6. Comparing Figures 18 and 19 with Figures 11 and 12 it is evident that carbide precipitation at the grain boundaries is significantly lower (Figure 19) or not present (Figure 18). Once again, as shown earlier from grainsize comparisons, the sensitization observed on Division I turbocharger bolts (Figures 11 and 12) are clearly attributable to the heat treatment process rather than to operational conditions.

Figure 20 is a micrograph of the washer and it shows a typical microstructure of A-286 material.

4.0 FRACTOGRAPHY

The broken bolt fracture surface was examined using a Scanning Electron Microscrop (SEM). Fractography was performed both on a as-received condition and a cleaned (removal of oxide layer using HCl) condition. The cleaning was necessary to identify fracture initiation, propagation and final failure. These areas are shown in Figure 2.

4.1 Pre-cleaning Fractography

Figure 21 is a fractograph taken at the mid-section of the granular fracture surface. It shows the grains and secondary cracks. The surface near the initiation site showed a similar appearance. Figure 22 is a fractograph at a higher magnification, in the same region, showing the individual grains, a secondary crack at grain boundary and the oxide layer covering the fracture surface. The oxide layer was

4.1 (CONTINUED)

very adherent typical of high temperature oxidation. Figure 23 is a fractograph taken in that region (predominantly shear, Figure 2) and shows evidence of a dimpled structure though the oxide layer blurs the clear evidence. Figure 24 is a fractograph taken at the lip region. The lip on the profile at the cut section plane (end view) showed a 45° drop. The shear lip is covered by oxide precluding a positive evidence of its presence. Based on the observations on the as-received surface it was decided to clean the surface in order to reveal the fractographic details that were not readily discernible. The surface was cleaned using a 50% solution of hydrochloric acid (HCl).

4.2 Post-Cleaning Fractography

Figures 25 through 29 show the fractographs of the fracture surface after it was cleaned. Figure 25 is taken near the edge where the crack initiated. The fracture surface shows the grains and secondary cracks. Comparing Figures 25 and 27, it is evident that the oxide layer has been removed and the underlaying metallic surface revealed. This initiation site is typical of intergranular stress corrosion cracking (IGSSC). Figure 26 is a fractograph taken in the wide region of the grainy morphology. This figure can be directly compared with Figure 21. Again, this is evidence of an IGSCC crack. Figure 27 is a fractograph taken in the transition region (see Figure 2 for location) where evidence of IGSCC and overload failure are both present. At this stage the IGSCC crack had propagated to a significant length whereby the preload in the bolt was being supported by a very small ligament area. Just adjacent to the transition zone is a region of pure ductile failure (see Figure 2 for location). This is shown in the fractograph in Figure 28. The dimpled structure, not clearly evident in Figure 23, is now obvious. This region marks the final stages of fracture of the bolt. The last stage of fracture was by a shear lip and this is shown in Figure 29. Once again, comparing

4.2 (CCONTINUED)

Figure 29 and Figure 24 it is clear that this region is better revealed after cleaning. Based on the fractographic observations it is evident that the crack initiated and propagated by IGSCC over a majority of the fracture area, converted to a mixed mode (IGSCC plus shear) when overload conditions were approached, to an overload ductile tearing mode and finally to a shear lip failure. This progression is approximately mapped in Figure 2.

5.0 CHEMICAL ANALYSIS

The purpose of chemical analysis was to:

1. Ascertain the bolt material specification since the material specification was unknown;

2. Identify the chemical species of the corrosion products on the fracture surface, within the grain boundaries, on the grain boundary and in the precipitates; and,

3. Identify the chemical species in the different colored corrosion products identified in the bolt and washers.

Item 1 was performed by wet chemistry techniques and items 2 and 3 using the energy dispersive x-ray fluorescence analysis feature in the SEM.

5.1 Bolt Material Chemical Analysis

The chemistry of the bolt as determined by wet gravimetric chemistry and typical composition from Reference 2 are provided below:

5.1 (CCONTINUED)

Chemisty (wt/%)

Element	As Determined	Per Reference 2
Chromium	13.69	15.0
Nickel	24.28	26.0
Molybdenum	1.02	1.25
Titanium	1.98	2.00
Vanadium	0.24	0.30
Silicon	0.23	-
Manganese	0.16	-
Aluminum	0.16	0.20
Copper	0.06	-
Phosphorous	0.013	-
Boron	0.004	.005
Sulphur	0.009	-
Carbon	0.042	0.04
Iron	Balance	55.2

Based on this comparison it was determined that the bolt material was A-286 stainless steel (iron-based precipitation hardening alloy) super alloy.

5.2 Chemical Identification Corrosion Products (Item 2)

The fracture surface of the broken bolt was analyzed in the SEM. The chemical species identified on the fracture surface are provided in Figure 30. Other than those attributable to the base metal, the presence of zinc, silicon, sulfur and calcium can be attributed to their presence in a typical fuel oil. The small sulfur peak indicates that the sulfur in the fuel oil was relatively low. At such low concentration of sulfur in combustion gases it is not conceivable that sulfidation could be the cause of IGSCC. Furthermore, per Reference

5.2 (CONTINUED)

3, for alloys with nickel concentration greater than 25 wt% and chromium less than 15 wt%, should sulfidation occur, the corrosion product would be predominantly nickel and sulfur (from NiS). This is because higher amounts of chromium would be necessary to preclude the formation of a low melting nickel sulfide eutectic. Also, Reference 3 provides a table for recommended maximum service temperatures in sulfur dioxide atmospheres for some selected stainless steels -- these temperatures range from 1292°F for a 410.S.S to 1850°F for 446.S.S. Considering this, it is not plausible that sulfidation could be the cause. In order to confirm the primary cause it was decided to identify the grain boundary corrosion product species. Figure 31 shows the identification of chemical species in the corrosion product shown in Figure 6. The corrosion product is predominantly iron with a notable absence of sulfur and very minute amounts of nickel. This would indicate that the corrosion product was predominantly iron oxide. Figure 32 shows the identification of the precipitate shown in Figure 7. The precipitate is primarily an intermetallic compound of titanium and molybdinum. Once again absence of sulfur is noted. Figure 33 identifies the product which appears as a white phase on the grain boundary in Figures 6 and 8. Figure 33 shows that the phase consists of species from the base metal itself. This is not believed to be a corrosion product. Figure 34 identifies the corrosion product within a grain boundary close to the fracture surface in Figure 4. Comparing this with Figure 31 shows the only difference being the presence of zinc in Figure 34. The minute amount of zinc was also observed in Figure 30 and believed to be from the combustion gases. The notable absence of sulfur and predominance of iron clearly shows the cause to be a high temperature oxidation mechanism. This observation is supported by articles in References 4 and 5 dealing with high temperature corrosion processes in stainless steels.

5.3 Chemical Identification of Corrosion Deposits (Items 3)

The corrosion products observed on the bolts and the washers were analyzed. The corrosion product on the washer was a biege colored deposit and the identification of species is provided in Figure 35. The species indicate that these are products of combustion of the fuel oil. The brown colored deposits on the head of the bolt is identified in Figure 36 and this spectrum is similar to the one from the washer. Comparing these two to that from the fracture surface (Figure 30) it is clear that the fracture surface did not contain the quantities present on the exposed surfaces. On one of the bolts, R-1 of Division II, a white deposit was observed in the fillet region between the shank and head of the bolt. Identification of this product is provided in Figure 37. This product had a significant quantity of copper. The amount of copper in the base metal (0.06 wt%) is not sufficient to show such a large peak. The presence of copper on this bolt's surface is unknown. However, the bolt did not show any evidence of pitting or cracking underneath this product. Therefore, the occurrence of copper in this deposit is not a cause for concern.

6.0 CONCLUSIONS

Based on the analysis, observations and evidence presented above, the following conclusions can be supported:

- Division I turbocharger bolts were found to have had a larger grain size than those of Division II and that the Division I bolts were sensitized (carbide at grain boundaries) indicating that the Division I bolts were improperly heat treated.

- Fractographic studies showed that the fracture was initiated and propagated by IGSCC, with ductile tearing and shear failure occurring during the final stages due to simple mechanical overload.

6.0 (CONTINUED)

- Analysis of the corrosion products within grain boundary cracks, the fracture surface, bolt head and washers clearly show the IGSCC to be caused by high temperature oxidation. Sulfidation mechanism is ruled out because:

  a. absence of sulfur in the corrosion products within grain boundaries;

  b. extremely small amount of sulfur on fracture surface as compared to the corrosion products on the bolt and washer; and

  c. the morphology of the fracture surface (granular versus sponge like appearances for sulfidation attack).

- IGSCC of the fractured bolts in Division I turbocharger occurred since these bolts were predisposed to this phenomenon by virtue of them being sensitized (improper heat treatment). Whereas the bolts from Division II were found to have had a proper heat treatment and no sensitization, hence did not experience any cracking though it had been in service for twice as long as those on Division I.

- A comparison between the microstructure of the Division I and Division II turbocharger bolts show that the larger grain size and sensitization of Division I bolt was not caused by operating temperatures. Instead it is heat treatment caused. Therefore, measuring turbocharger inlet temperature may not be meaningful to the present cause.

7.0 REFERENCES

1. "Metallography, Structures and Phase Diagrams", Vol. 8, Metals Handbook, Eighth Edition, American Society for Metals, Metals Park, Ohio.

2. "Properties and Selection: Stainless Steels, Tool Materials and Special Purpose Metals", Metals Handbook Vol. 3, Ninth Edition, American Society for Metals, Metals Park, Ohio.

3. "Handbook of Stainless Steels", D. Peckner and I. M. Bernstein, Editors, McGraw Hill.

4. "Source Book on Materials for Elevated Temperature Applications", E. F. Bradley, Editor, American Society for Metals, Metals Park, Ohio.

5. "Super Alloys - Source Book", M. J. Donachie, Jr., Editor, American Society for Metals, Metals Park, Ohio.

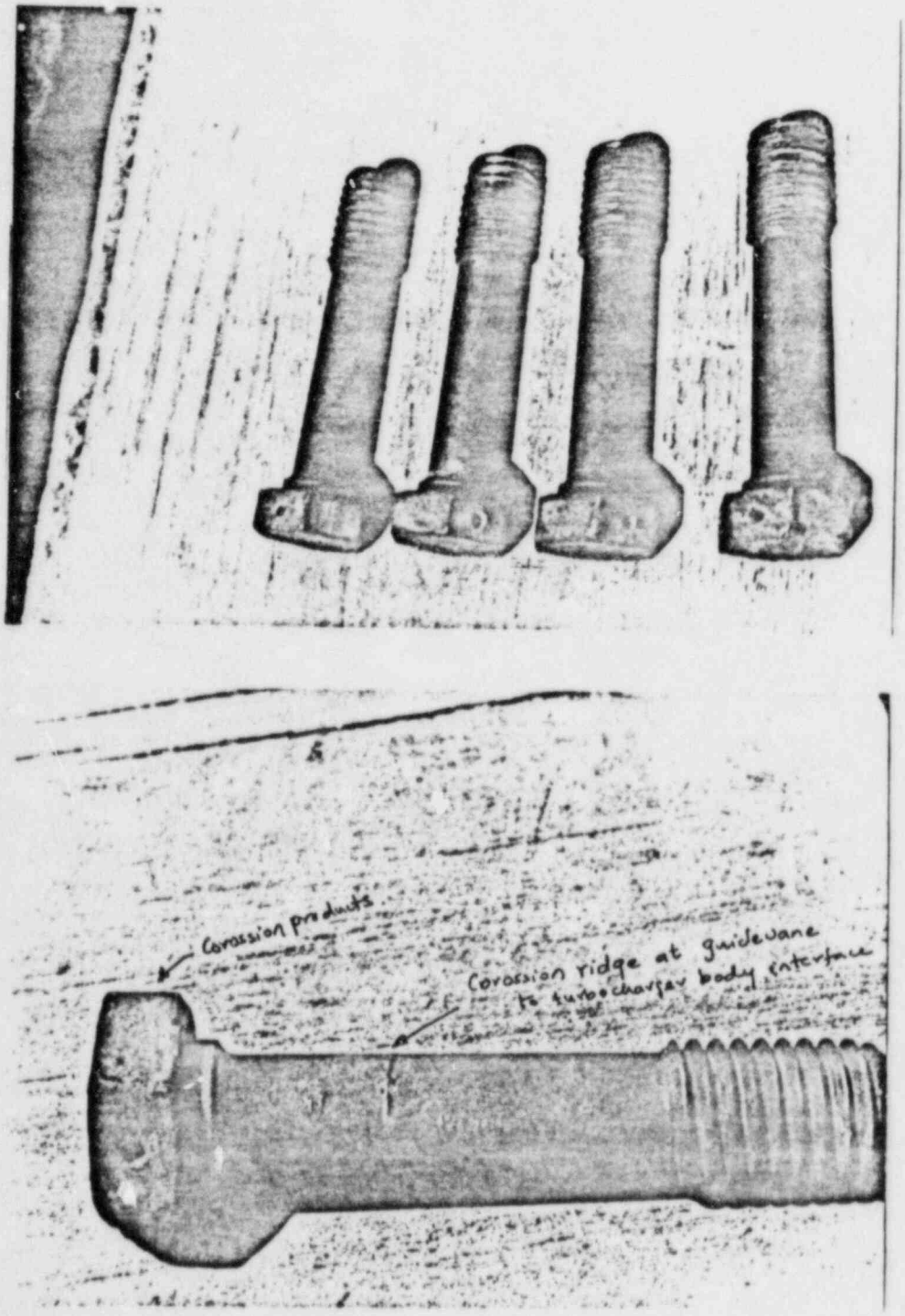

Figure 1 As-received Turbocharger Bolts From Division I

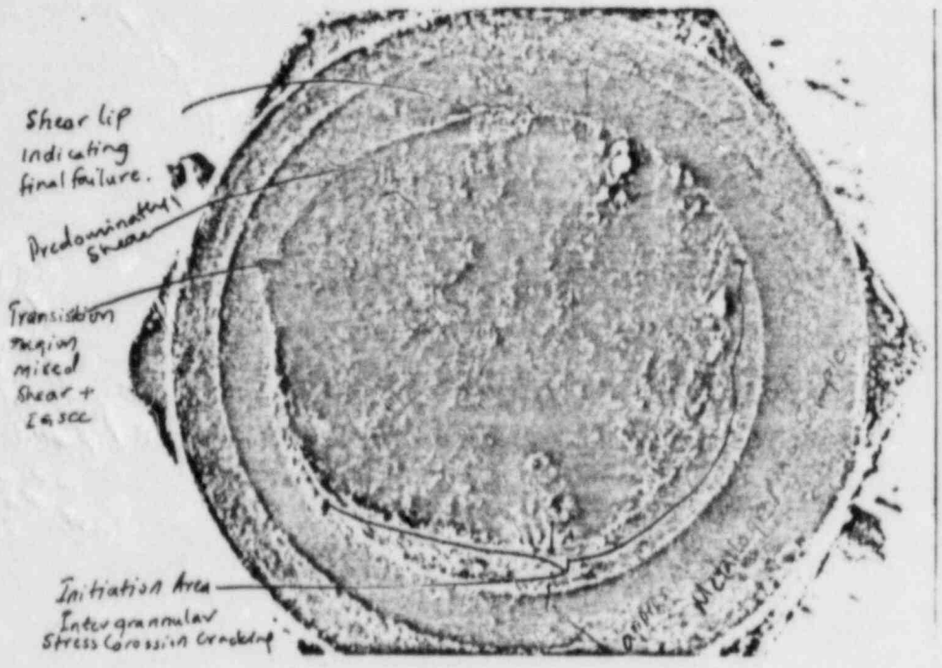

Figure 2 As-received Fracture Surface of Broken Bolt From Division I

Shows where specimen for metallography was obtained. The areas of fracture initiation and propagation were marked based on fractographic evaluation presented in Section 4.0.

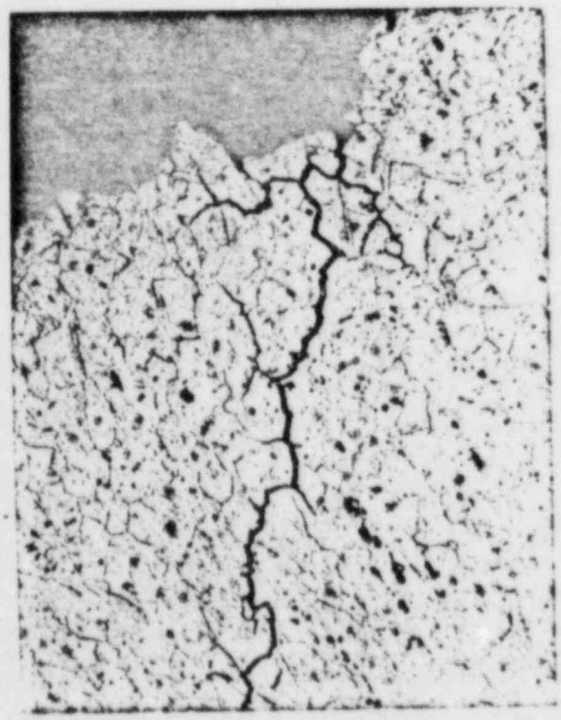

Etchant: 10% Oxalic Acid
Electolytic Etch

Magnification: 100x

Figure 3 Integranular Crack at Fracture Surface

Crack follows grain boundaries showing a typical IGSCC appearance. Inclusion like islands in the matrix are Intermetallic Compound precipitates.

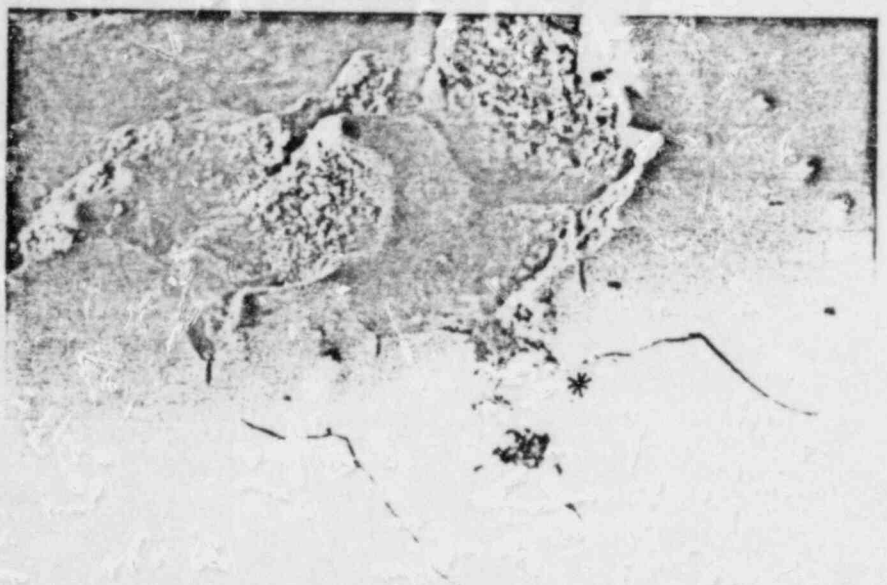

Etchant: 10% Oxalic Acid
Electrolytic Etch

Magnification: 500x

Figure 4 SEM Metallograph at Fracture Surface

Grains on fracture surface and a secondary crack are visible. The cracks on polished face are branches from a main secondary crack that emanates to the fracture surface. The main secondary crack is not on the observed plane.

* denotes area for chemical identification

Etchant: 10% Oxalic Acid
Electrolytic Etch

Magnification: 500x

Figure 5 SEM Metallograph at Fracture Surface Intergranular Cracking

Appearance similar to Figure 4.

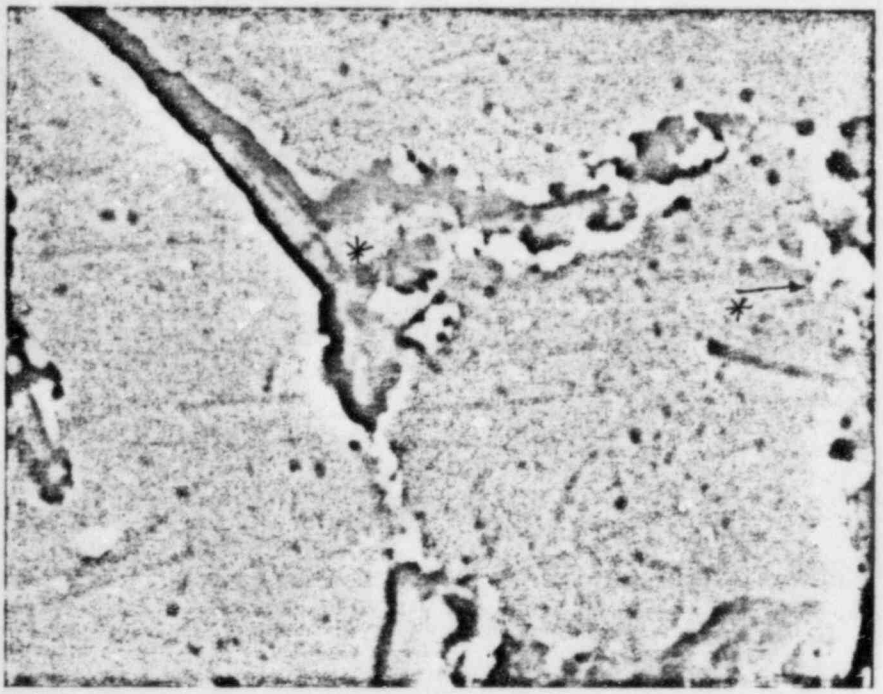

Etchant: 10% Oxalic Acid
Electrolytic Etch

Magnification: 5000x

Figure 6 SEM Metallograph

Corrosion Product (Iron Oxide) in Grain Boundaries (Division I)

Corrosion product within grain boundary crack clearly visible. Also visible is a white phase segregation along grain boundary.

* denotes chemical identification area

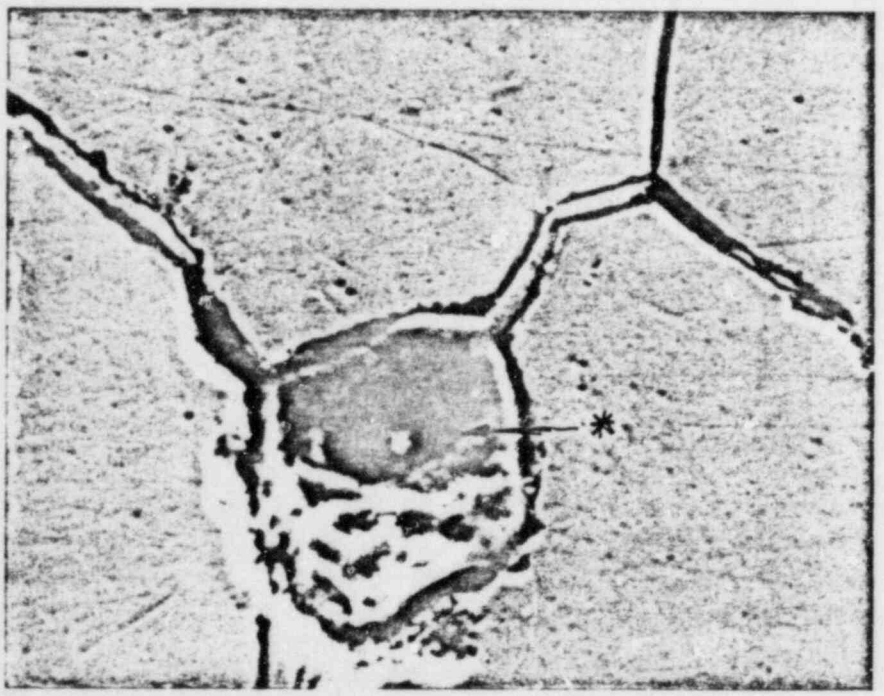

Etchant: 10% Oxalic Acid
Electrolytic Etch

Magnification: 2000x

Figure 7 SEM Metallograph of Inclusion

Inclusion was found to be an intermetallic compound precipitate formed during aging treatment. Precipitate was a Titanium-Molybdenum Intermetallic Compound.

* denotes chemical identification spot

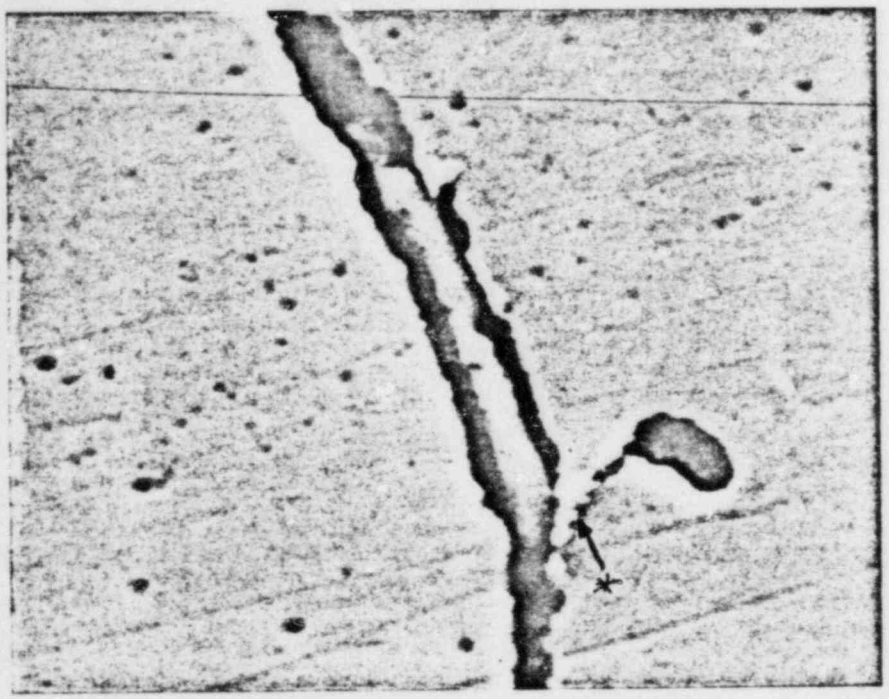

Etchant: 10% Oxalic Acid
Electrolytic Etch

Magnification: 5000x

Figure 8 SEM Metallograph of Intergranular Corrosion Product

Nickel rich phase along grain boundary.

* denotes chemical identification spot

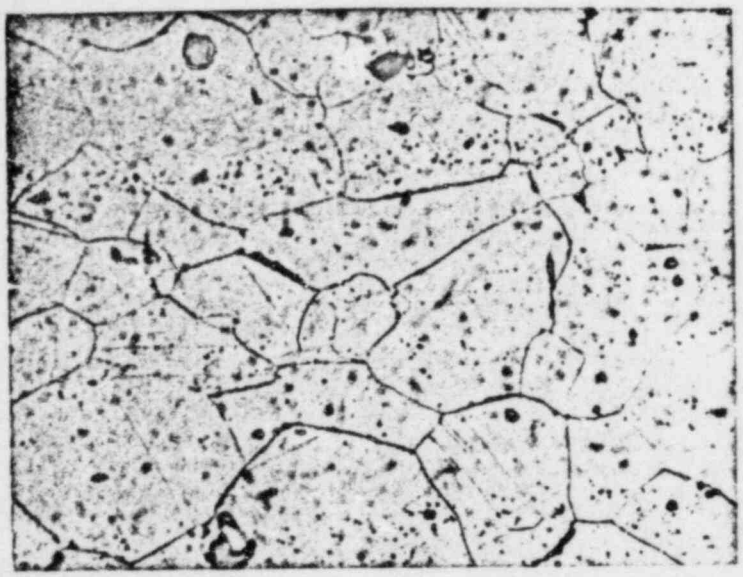

Etchant: 10% Oxalic Acid
Electrolytic Ecch

Magnification: 400x

Figure 9 Photomicrograph of Broken Turbocharger Bolt (Division I)

Note large grains and intermetallic precipitates. There is some evidence of grain boundary precipitation.

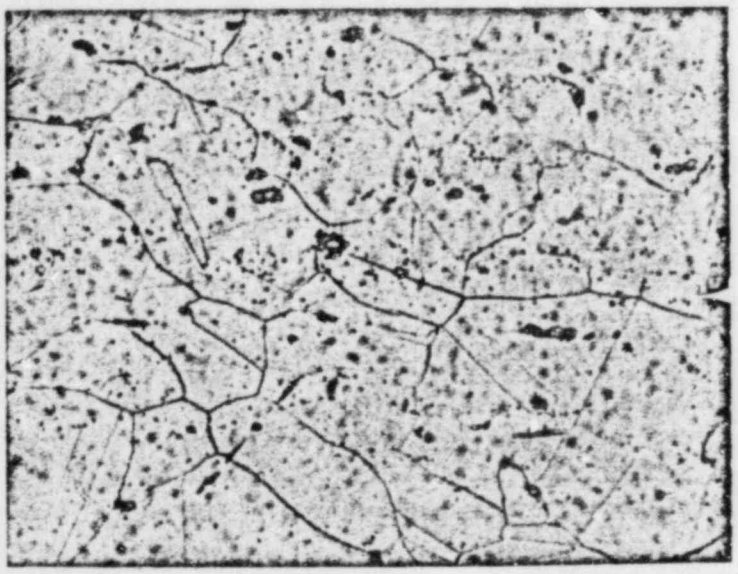

Etchant: 10% Oxalic Acid
Electrolytic Etch

Magnification: 400x

Figure 10 Photomicrograph of Unbroken Turbocharger Bolt (Division I)

Large grains, intermetallic precipitates and grain boundary precipitates.

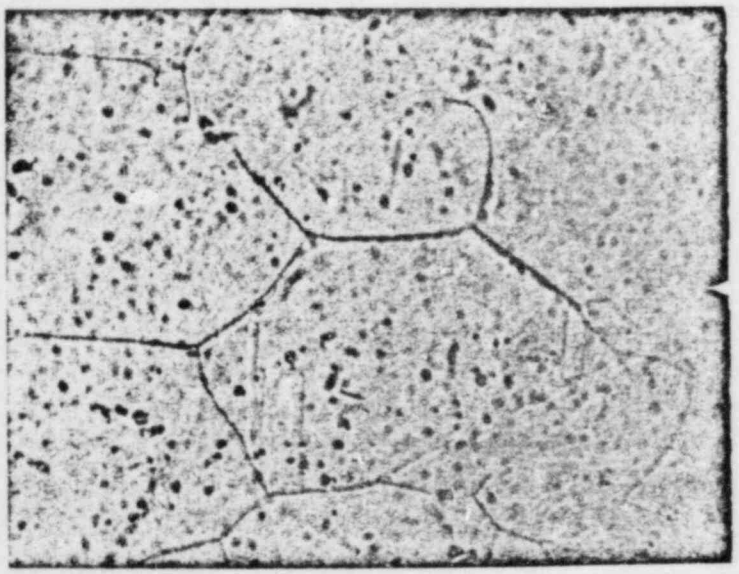

Etchant: 10% Oxalic Acid
Electrolytic Etch

Magnification: 800x

Figure 11 Photomicrograph of Broken Turbocharger Bolt (Division I)

Note grain boundary precipitation, indicating sensitization of bolt material.

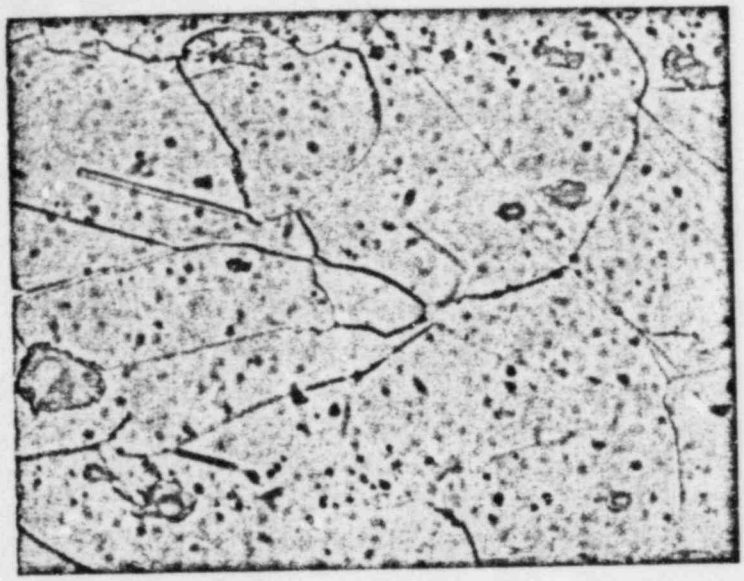

Etchant: 10% Oxalic Acid
Electrolytic Etch

Magnification: 800x

Figure 12 Photomicrograph of Unbroken Turbocharger Bolt (Division I)

Note grain boundary precipitation. Indicates sensitization of bolt material.

Etchant: 10% Oxalic Acid
Electrolytic Etch

Magnification: 500x

Figure 13 Photomicrograph of New Unused A-286 Bolt

Small ç ains. No evidence of grain boundary precipitation.

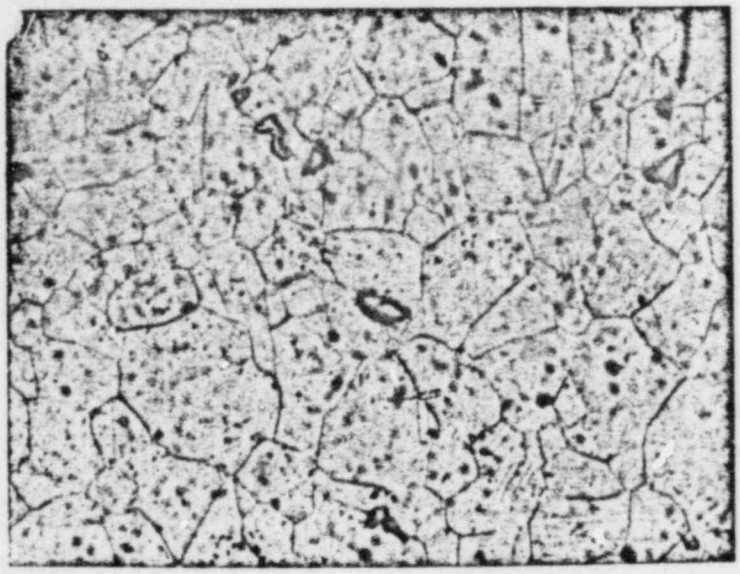

Etchant: 10% Oxalic Acid
Electrolytic Etch

Magnification: 400x

Figure 14 Photomicrograph of Turbocharger Bolt From Division II L-1 Bolt

Note smaller grain size than the Division I bolts. Microstructure shows some evidence of stepping, indicating absence of sensitization.

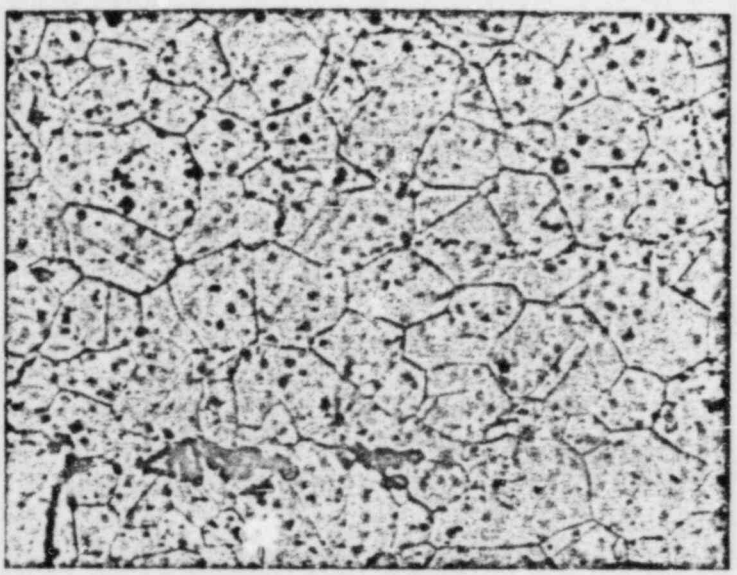

Etchant: 10% Oxalic Acid
Electrolytic Etch

Magnification: 400x

Figure 15 Photomicrograph of Turbocharger Bolt From Division II L-3 Bolt
(Same as figure 14)

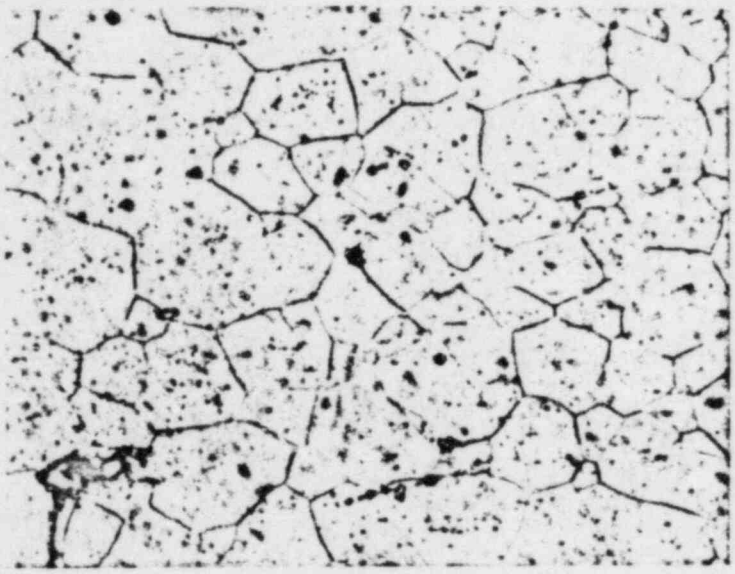

Etchant: 10% Oxalic Acid
Electrolytic Etch

Magnification: 400x

Figure 16 Photomicrograph of Turbocharger Bolt From Division II R-2 Bolt

(Same as figure 14)

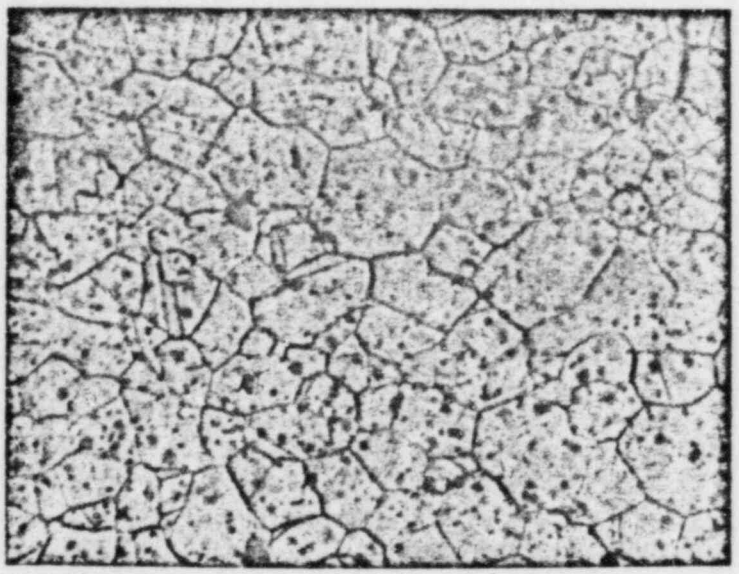

Etchant: 10% Oxalic Acid
Electrolytic Etch

Magnification: 400x

Figure 17 Photomicrograph of Turbocharger Bolt From Division II R-6 Bolt

(Same as figure 14)

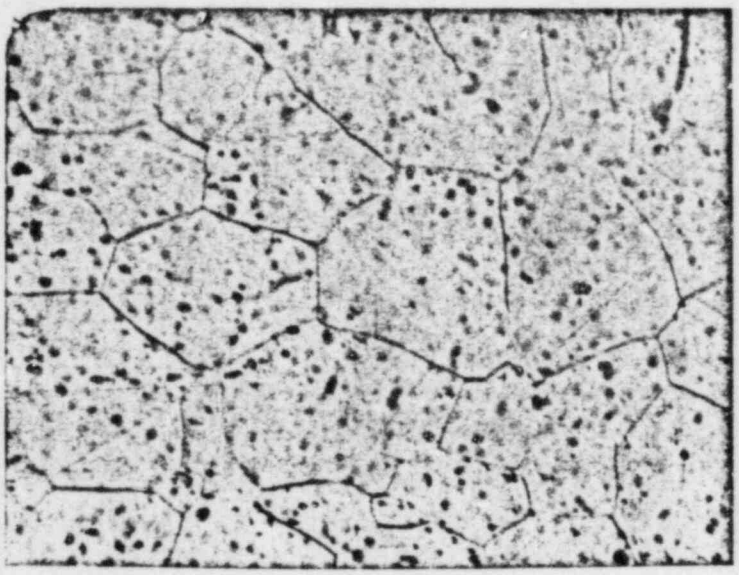

Etchant: 10% Oxalic Acid
Electrolytic Etch

Magnification: 800x

Figure 18 Photomicrograph of Turbocharger Bolt From Division II L-3 Bolt

Note absence of grain boundary precipitation. Material was not sensitized.

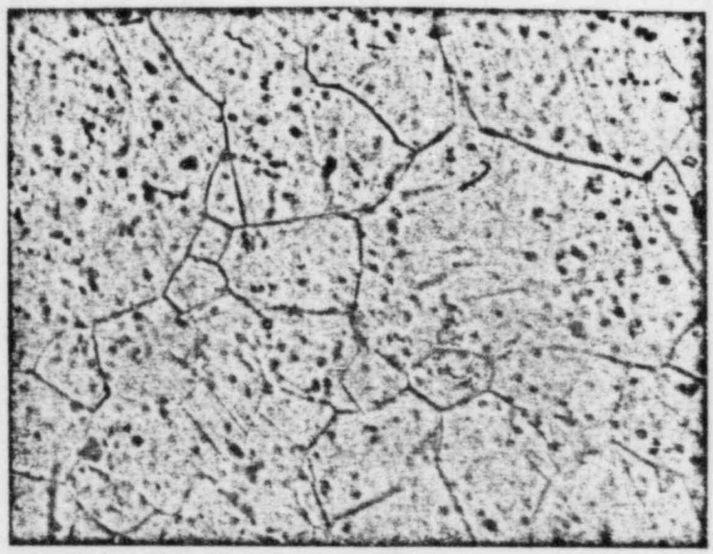

Etchant: 10% Oxalic Acid
Electrolytic Etch

Magnification: 800x

Figure 19 Photomicrograph of Turbocharger Bolt From Division II

Very slight evidence grain boundary precipitation. Material is not sensitized.

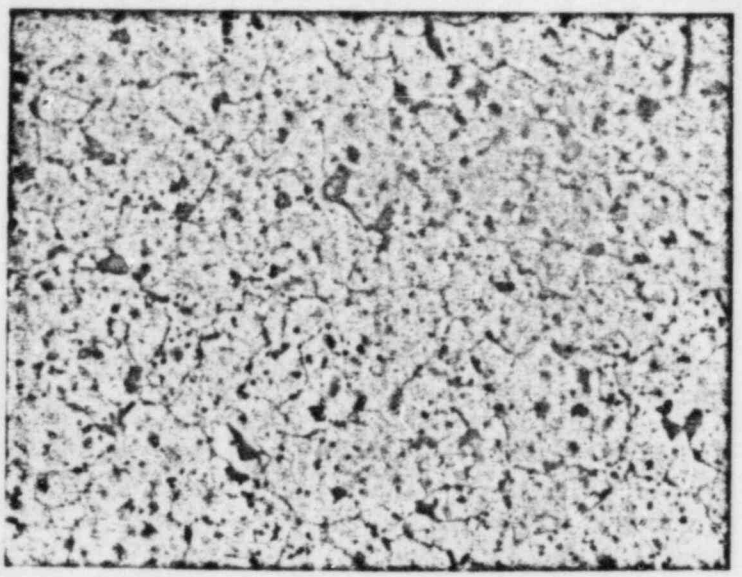

Etchant: 10% Oxalic Acid
Electrolytic Etch

Magnification: 400x

Figure 20 Photomicrograph of Washer From Division II Turbocharger Bolt

Typical A-286 microstructure.

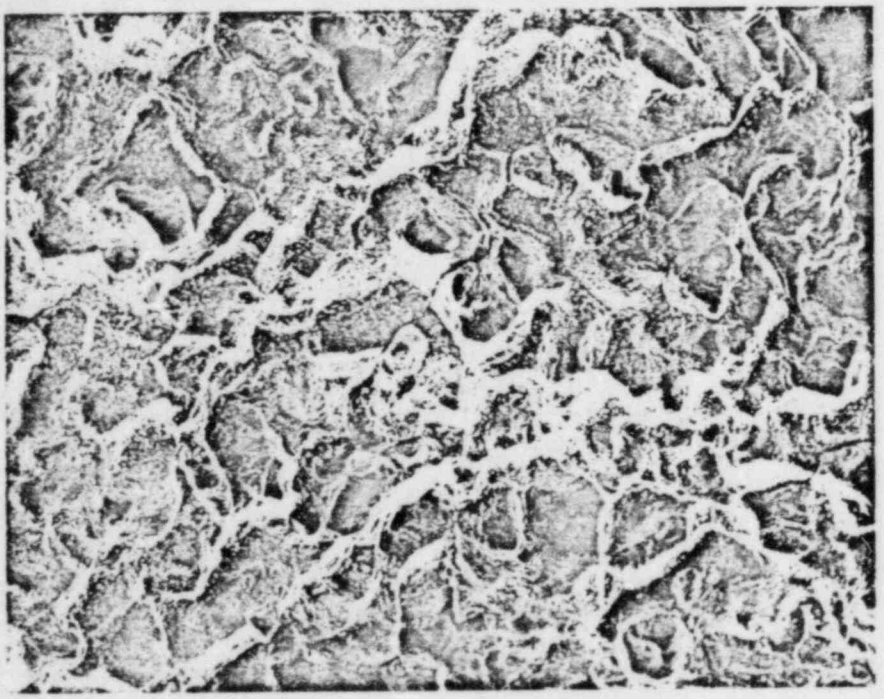

Magnification: 200x

Figure 21 SEM Fractograph - Division I Broken Bolt Head

Individual grains and secondary cracks are visible.
Surface covered with an oxide layer.

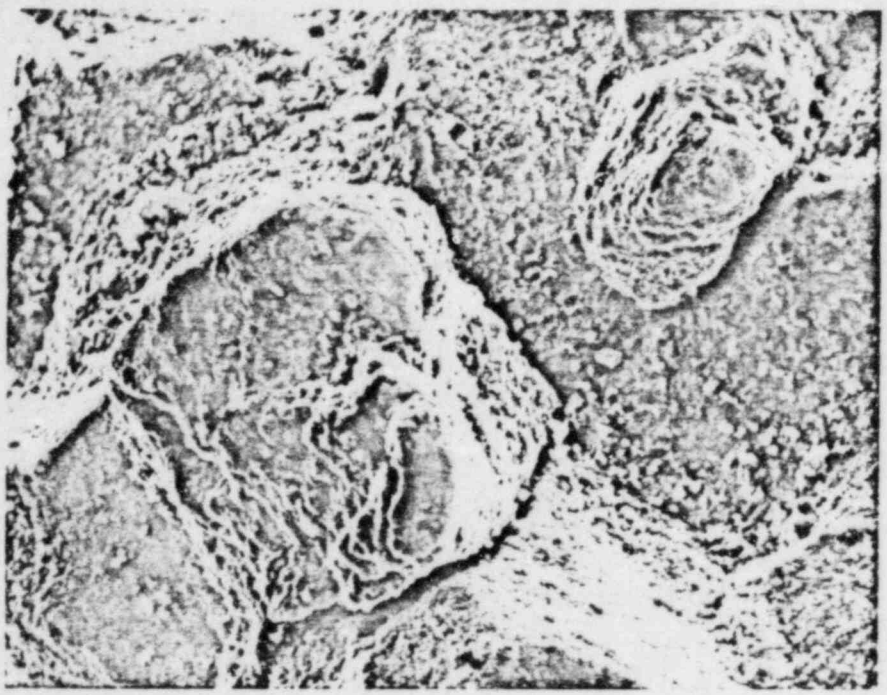

Magnification: 900x

Figure 22 SEM Fractograph - Division I Broken Bolt Head

At higher magnification secondary crack, austenite grains and oxide layer are clearly visible.

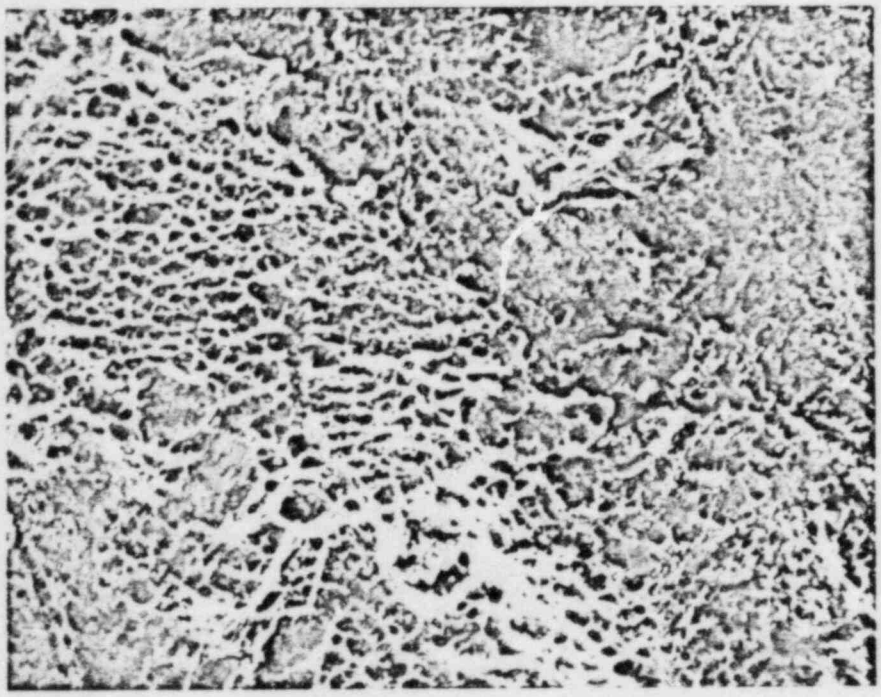

Magnification: 1000x

Figure 23 SEM Fractograph - Division I Broken Bolt Head

Taken near the smooth appearing region in Figure 2. Appearance of ductile tearing due to mechanical overload is blurred by oxide film.

Magnification: 50x

Figure 24 SEM Fractograph - Division I Broken Bolt Head

Area near shear lip. Appearance of shear blurred by oxide film.

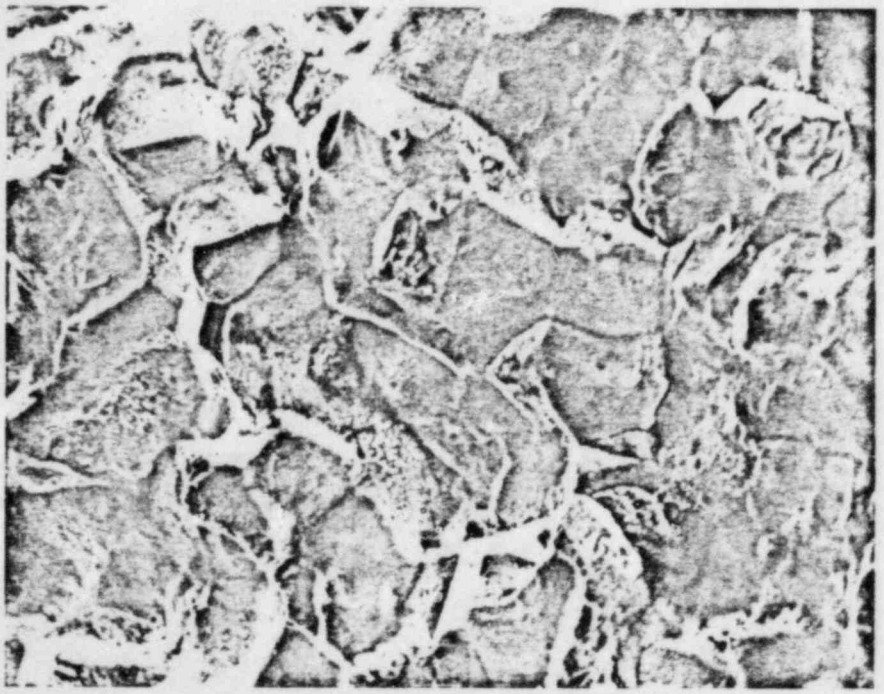

Magnification: 450x

Figure 25 SEM Fractograph - Division I Broken Bolt Head

(After cleaning)

Fractograph taken near initiation point. Clear evidence that IGSCC initiated cracking.

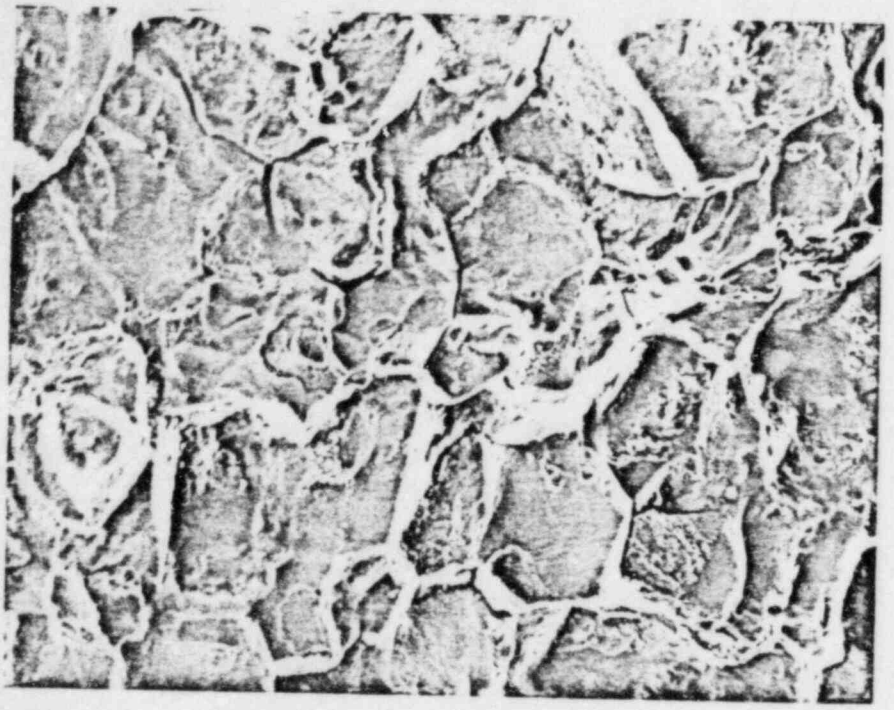

Magnification: 400x

Figure 26 SEM Fractograph - Division I Broken Bolt Head

(After cleaning)

Fractograph taken in the mid-region of grainy surface. Evidence of IGSCC is clear.

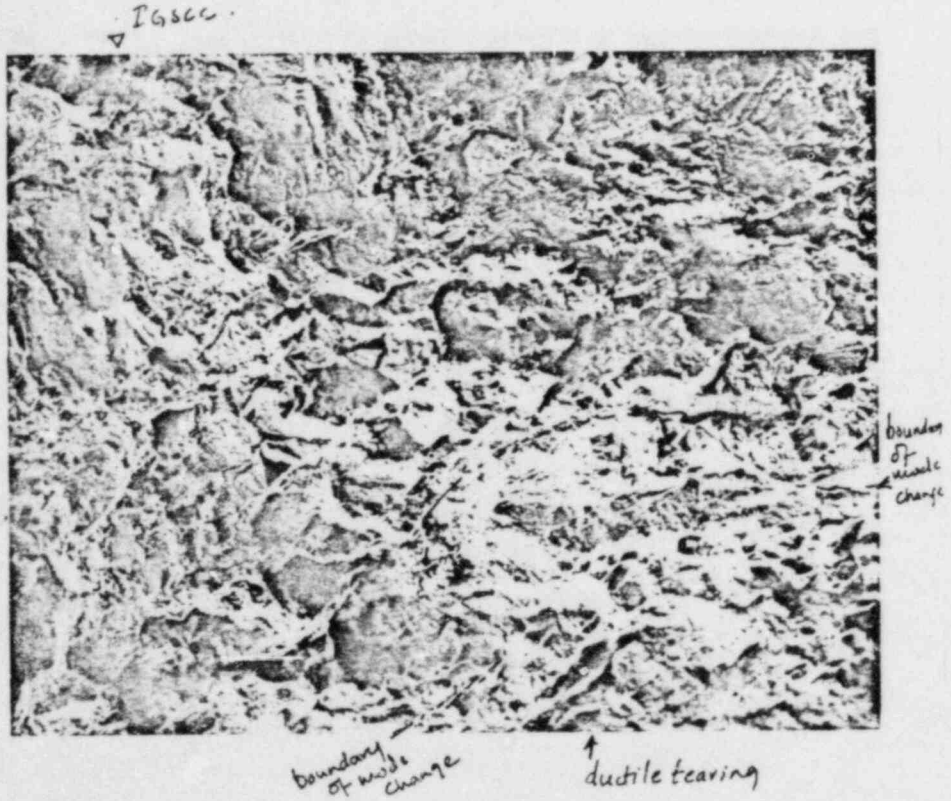

Magnification: 200x

Figure 27 SEM Fractograph - Division I Broken Bolt Head

(After cleaning)

Fractograph taken at transition region between grainy surface and smooth surface. Evidence of IGSCC (grains and secondary cracks) at upper half and ductile tearing at lower right.

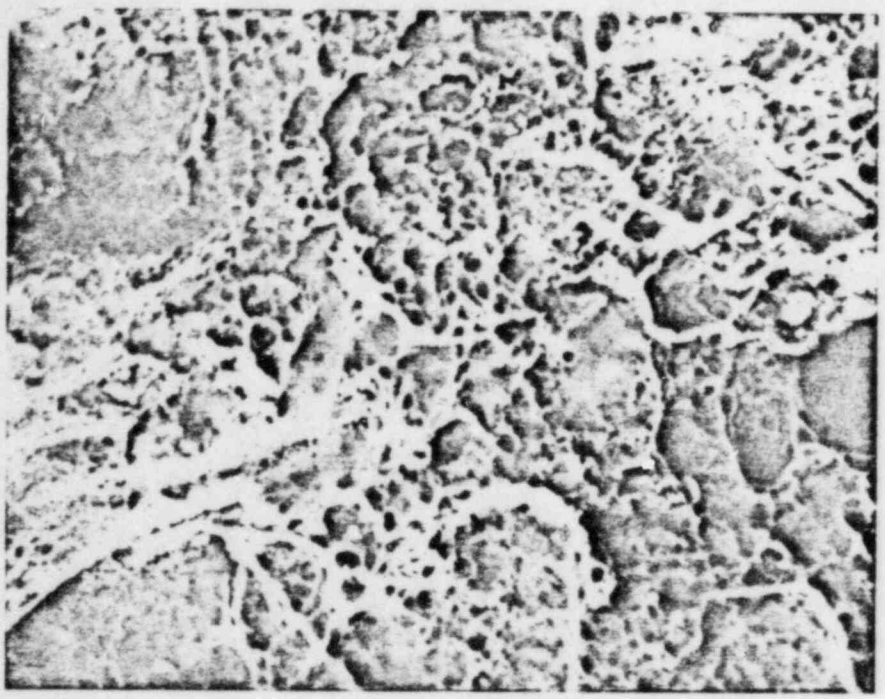

Magnification: 160x

Figure 28 SEM Fractograph - Division I Broken Bolt Head

(After cleaning)

Taken in the smooth region in Figure 2. Dimpled morphology typical of ductile tearing due to mechanical overload.
(Preload supported by a small ligament area)

Magnification: 40x

Figure 29 SEM Fractograph - Division I Broken Bolt Head

(After cleaning)

Shear lip formation is evident. Indicates the last step of fracture.

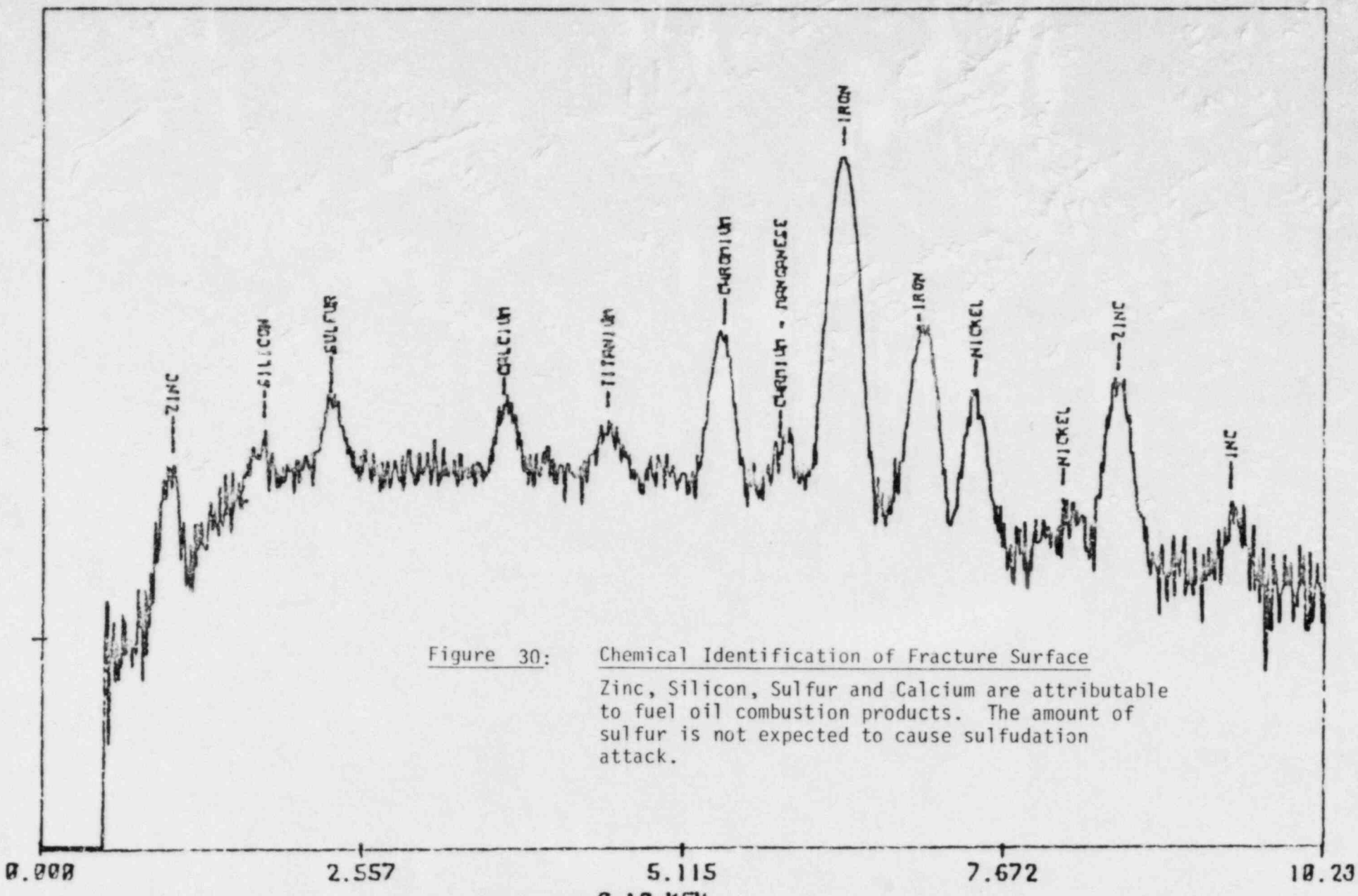

Figure 30: Chemical Identification of Fracture Surface

Zinc, Silicon, Sulfur and Calcium are attributable to fuel oil combustion products. The amount of sulfur is not expected to cause sulfudation attack.

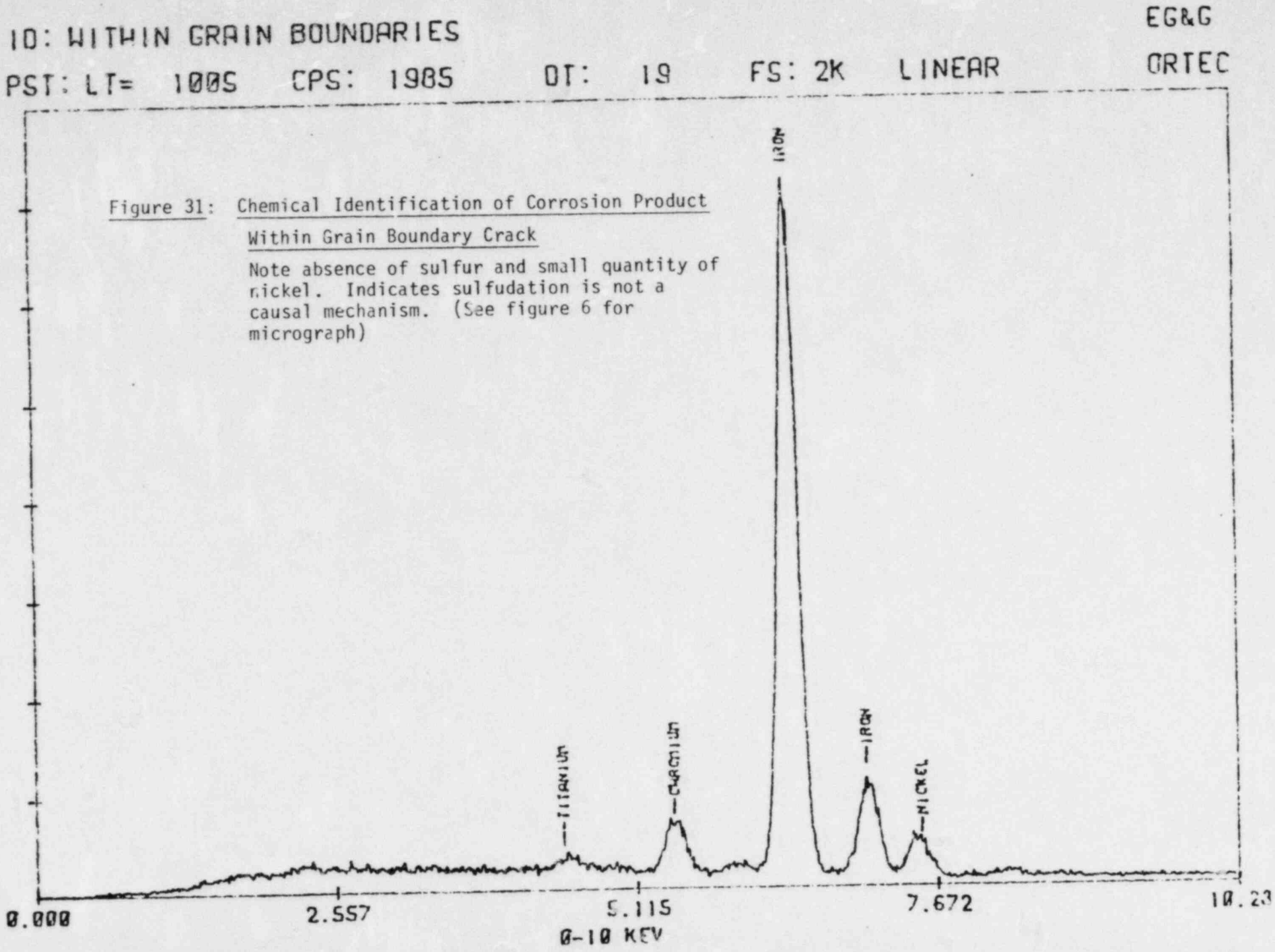

Figure 31: Chemical Identification of Corrosion Product Within Grain Boundary Crack

Note absence of sulfur and small quantity of nickel. Indicates sulfudation is not a causal mechanism. (See figure 6 for micrograph)

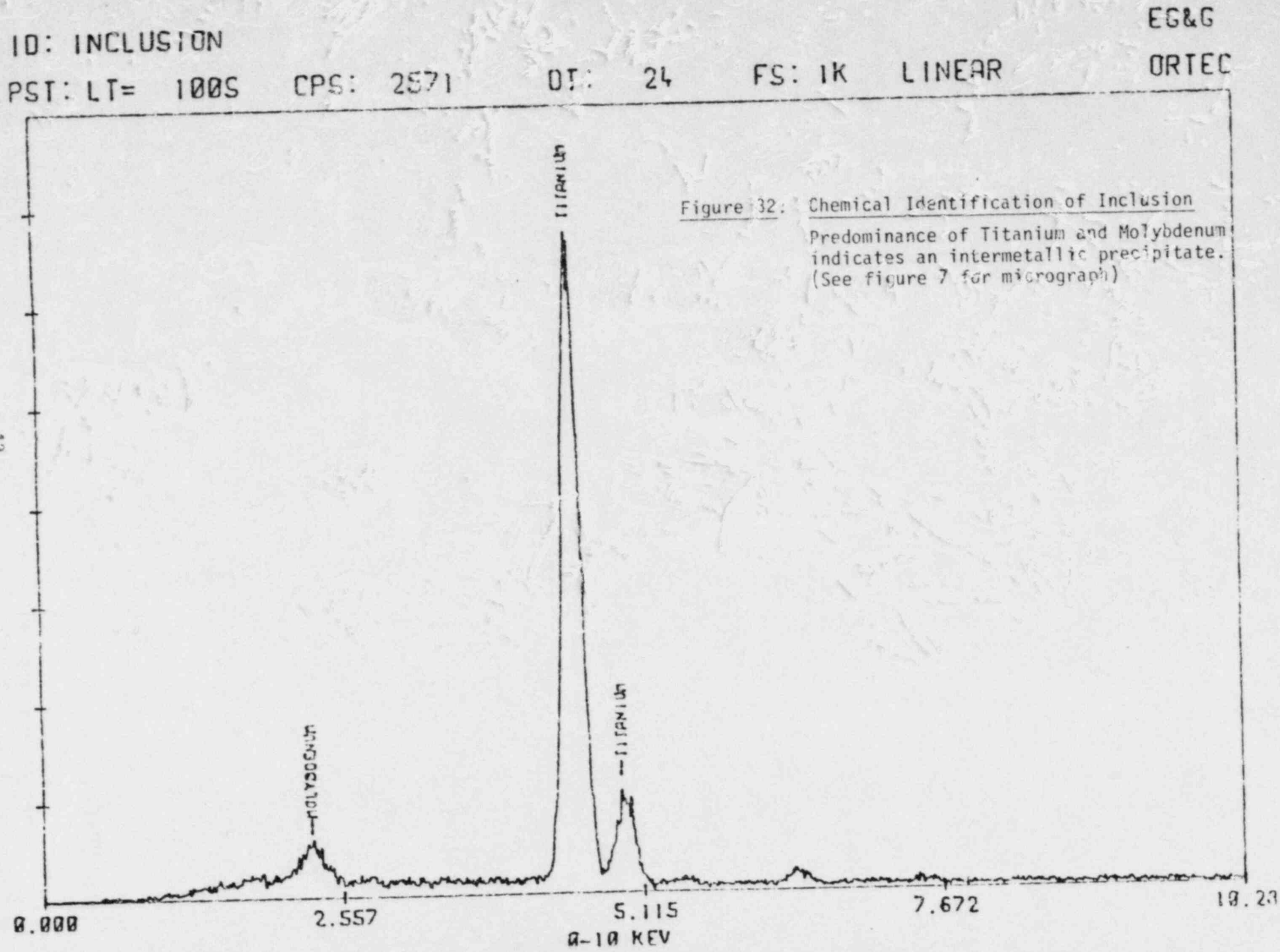

Figure 32: Chemical Identification of Inclusion

Predominance of Titanium and Molybdenum indicates an intermetallic precipitate. (See figure 7 for micrograph)

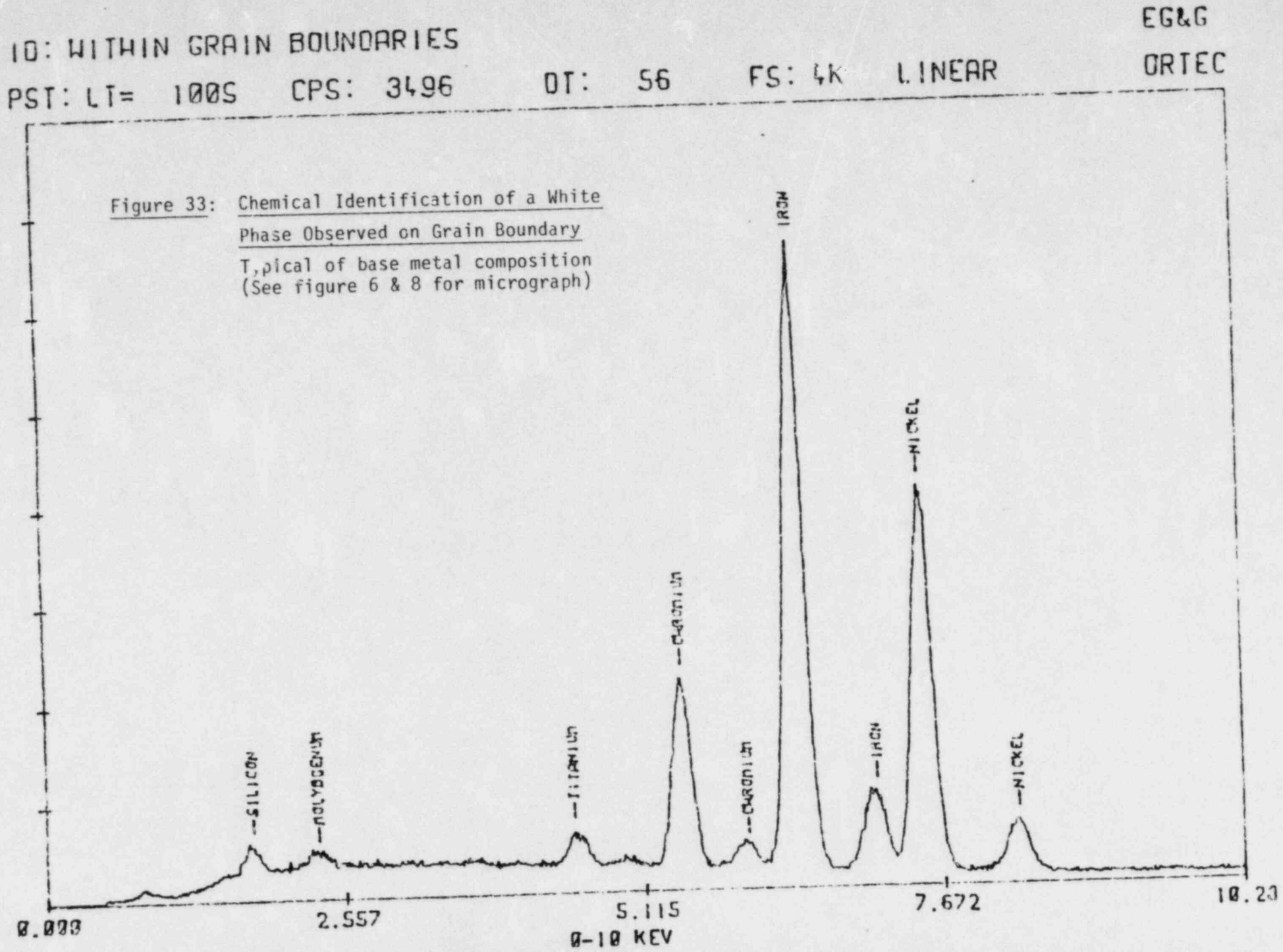

Figure 33: Chemical Identification of a White Phase Observed on Grain Boundary

T,pical of base metal composition
(See figure 6 & 8 for micrograph)

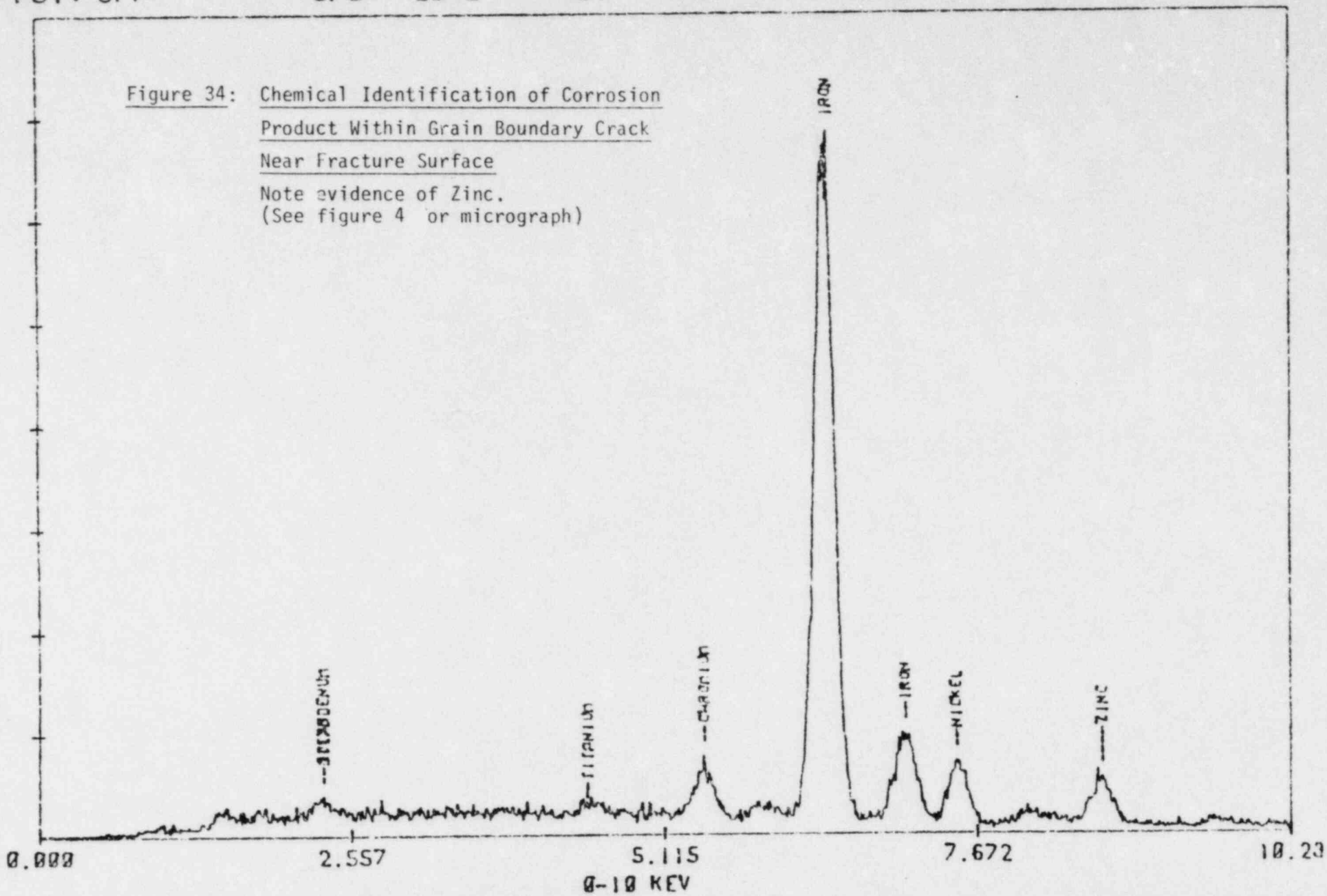

Figure 34: Chemical Identification of Corrosion Product Within Grain Boundary Crack Near Fracture Surface

Note evidence of Zinc.
(See figure 4 or micrograph)

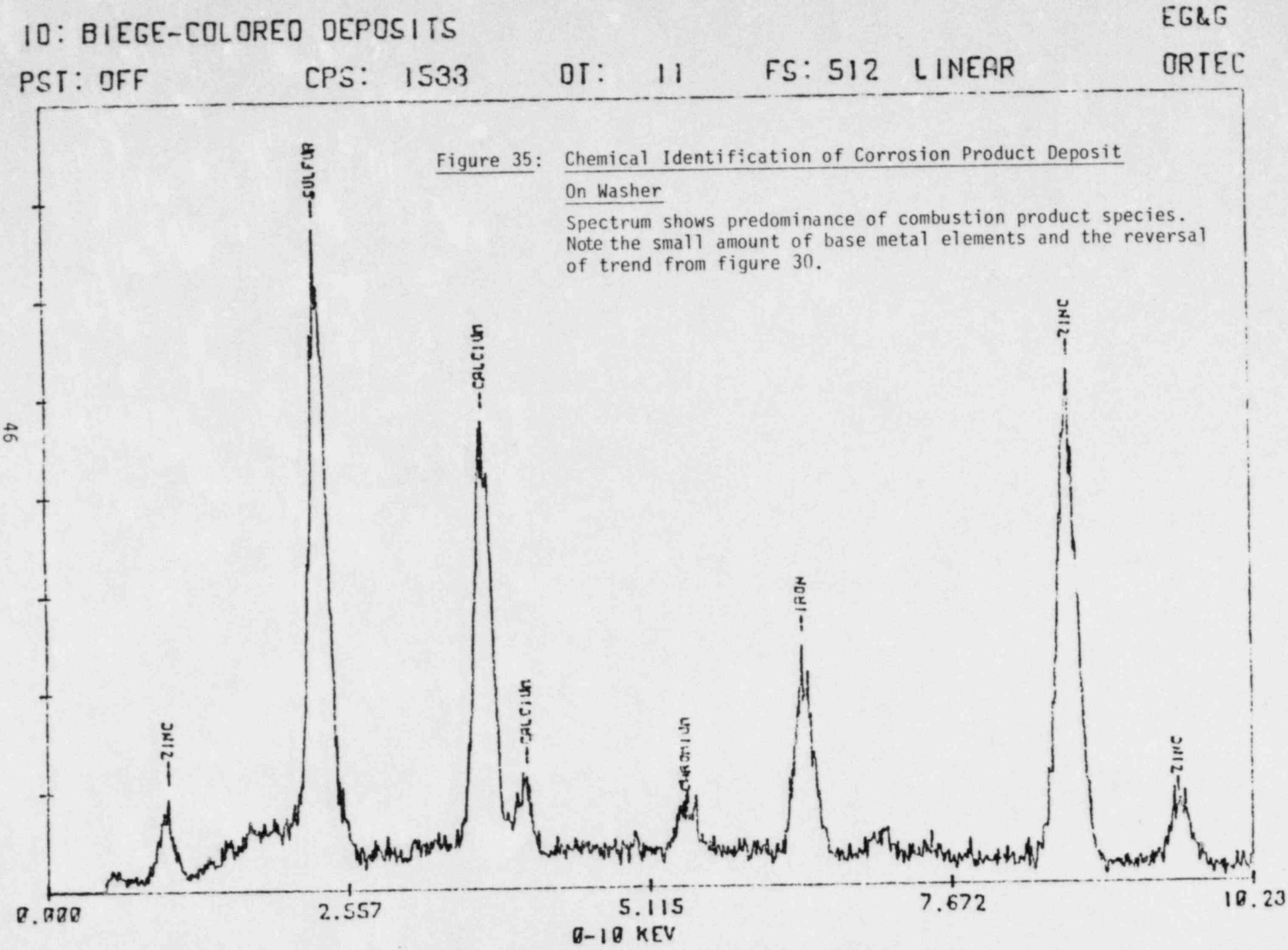

Figure 35: Chemical Identification of Corrosion Product Deposit On Washer

Spectrum shows predominance of combustion product species. Note the small amount of base metal elements and the reversal of trend from figure 30.

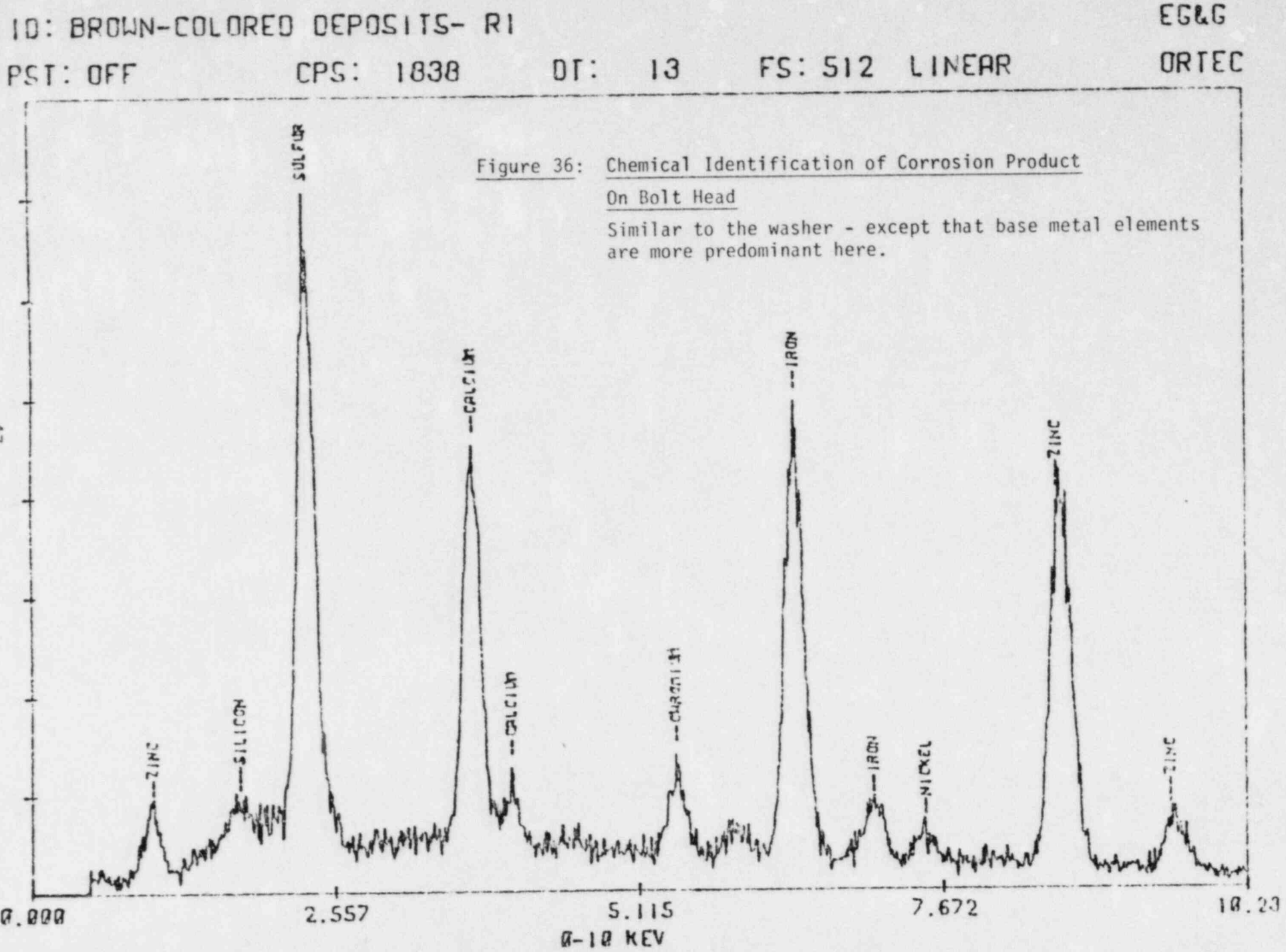

Figure 36: Chemical Identification of Corrosion Product On Bolt Head

Similar to the washer - except that base metal elements are more predominant here.

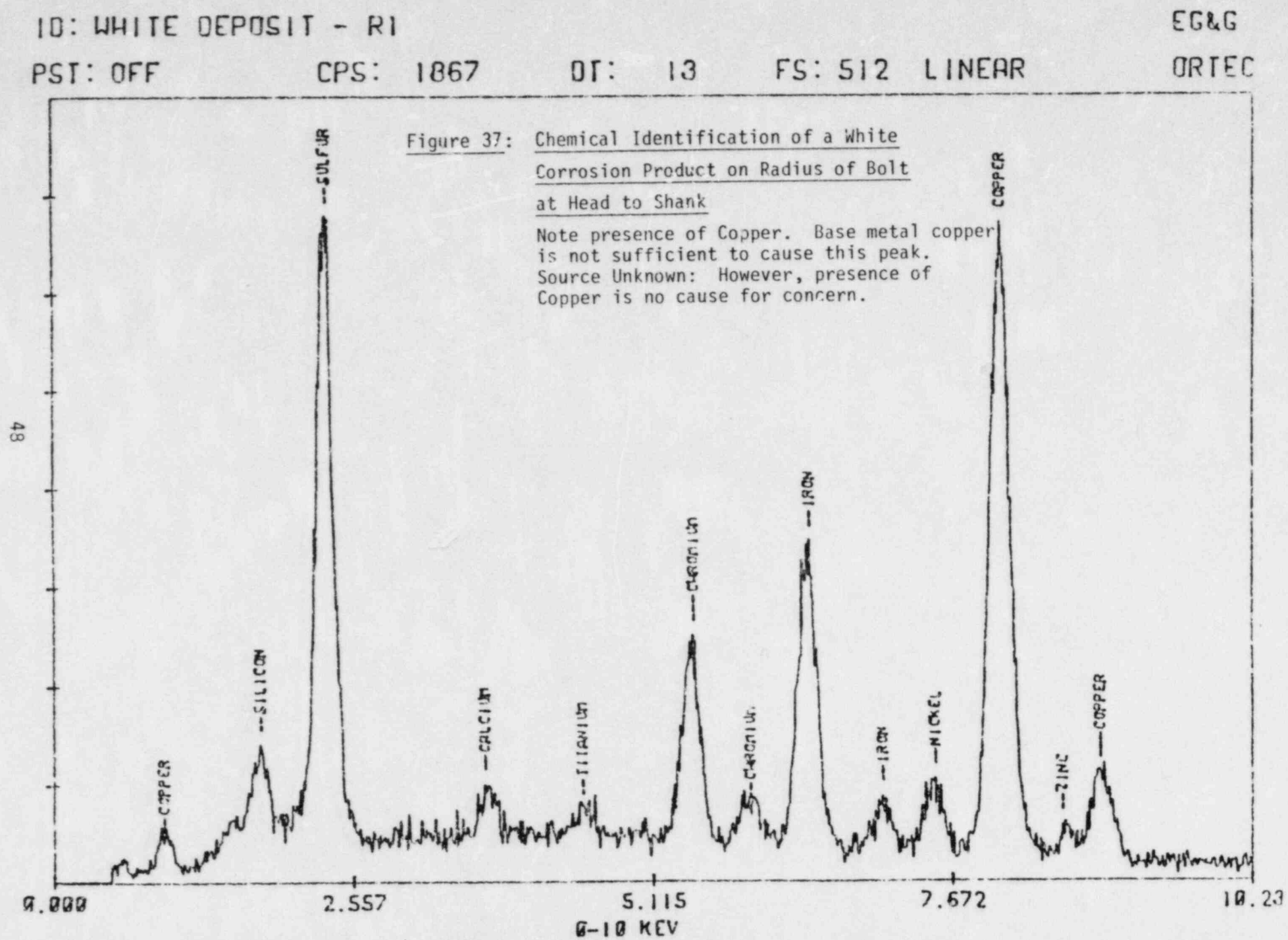

Figure 37: Chemical Identification of a White Corrosion Product on Radius of Bolt at Head to Shank

Note presence of Copper. Base metal copper is not sufficient to cause this peak. Source Unknown: However, presence of Copper is no cause for concern.